

# Toxicity Evaluations of Superparamagnetic Iron Oxide Nanoparticles: Cell “Vision” *versus* Physicochemical Properties of Nanoparticles

Morteza Mahmoudi,<sup>†,‡,\*</sup> Sophie Laurent,<sup>§</sup> Mohammad A. Shokrgozar,<sup>†</sup> and Mohsen Hosseinkhani<sup>||,\*</sup>

<sup>†</sup>National Cell Bank, Pasteur Institute of Iran, Tehran, 1316943551 Iran, <sup>‡</sup>Nanotechnology Research Centre, Faculty of Pharmacy, Tehran University of Medical Sciences, Tehran, Iran, <sup>§</sup>Department of General, Organic, and Biomedical Chemistry, NMR and Molecular Imaging Laboratory, University of Mons, Avenue Maistriau, 19, B-7000 Mons, Belgium, <sup>||</sup>Cardiovascular Research Center, Mount Sinai School of Medicine, New York, New York 10029, United States, and <sup>||</sup>National Institute of Genetic Engineering and Biotechnology (NIGEB), Tehran, Iran

**S**uperparamagnetic iron oxide nanoparticles (SPIONs) have great potential for a wide use in various biomedical applications, including magnetic resonance imaging (e.g., as contrast agents),<sup>1</sup> drug delivery,<sup>2</sup> hyperthermia,<sup>3</sup> transfections,<sup>4</sup> *in vivo* cell tracking,<sup>1</sup> and tissue repair.<sup>5</sup> Research involving the use of SPIONs with various surface chemistries continues to evolve with their growth for human *in vivo* applications. Although only dextran-coated SPIONs are approved for human *in vivo* use by the Food and Drug Administration (FDA),<sup>2</sup> several SPIONs with various physicochemical properties are in clinical trials; so, one can expect that several SPIONs will be utilized in many more commercial products for various biomedical applications in the not-too-distant future.<sup>6</sup>

Therefore, biological issues in relation to SPIONs have been increasingly addressed in the past few years, and toxicity has clearly become an important one. In order to achieve deep understanding of the toxicity pathways of various SPIONs, crucial for their safe use in humans, a great amount of reliable research must be conducted at present; a significant knowledge gap exists on a complete toxicological profile of SPIONs, and there is urgent need for risk assessment and safety regulations of SPIONs.

A precise analysis of the literature shows conflicting results on the toxicity of nanomaterials and specifically of SPIONs. For instance, Karlsson *et al.*<sup>7</sup> evaluated the toxicity of bare SPIONs on human lung epithelial cell line (*i.e.*, A549) and found that there

**ABSTRACT** In the last few decades, nanoparticles (NPs) have been recognized as promising candidates for starting a new revolution in science and technology due to their unusual properties, attracting the attention of physicists, chemists, biologists, and engineers. The aim of this study is to evaluate the toxicities (at both cellular and molecular levels) of three forms of superparamagnetic iron oxide nanoparticles (SPIONs) of various surface chemistries (COOH, plain, and NH<sub>2</sub>) through the comparison with gene expression patterns of three cell types (*i.e.*, human heart, brain, and kidney). For this purpose, both an MTT assay and a DNA microarray analysis were applied in three human cell lines—HCM (heart), BE-2-C (brain), and 293T (kidney)—under the exposure to SPIONs-COOH, SPIONs-NH<sub>2</sub>, and bare SPIONs. The specific gene alteration and hierarchical clustering revealed that SPIONs-COOH altered genes associated with cell proliferative responses due to their reactive oxygen species (ROS) properties. It was also found that the cell type can have quite a significant role in the definition of suitable pathways for detoxification of NPs, which has deep implications for the safe and high yield design of NPs for biomedical applications and will require serious consideration in the future.

**KEYWORDS:** toxicity · superparamagnetic iron oxide nanoparticles' cell “vision” · physicochemical properties

was no or low toxicity of SPIONs at the applied concentrations (20–80  $\mu$ g/mL), while in other studies, bare SPIONs showed severe toxicity at the same concentration on human fibroblast.<sup>8,9</sup> In addition, there was no trace of bare SPION toxicity on mouse fibroblast cells even at higher concentrations (500  $\mu$ g/mL).<sup>10–12</sup> There are plenty of additional examples of contradictory reports on the toxicity of particles when the exact same nanoparticles (SPIONs) were interacted with various cells.<sup>13–30</sup> We postulate that these significant differences between results may be related to the different detoxification approaches that the cells use for toleration/fight against NPs.

\* Address correspondence to mohsen.hosseinkhani@mssm.edu, mohmoudi@biospion.com, Web: www.biospion.com.

Received for review June 8, 2011 and accepted August 14, 2011.

Published online August 15, 2011  
10.1021/nn2021088

© 2011 American Chemical Society

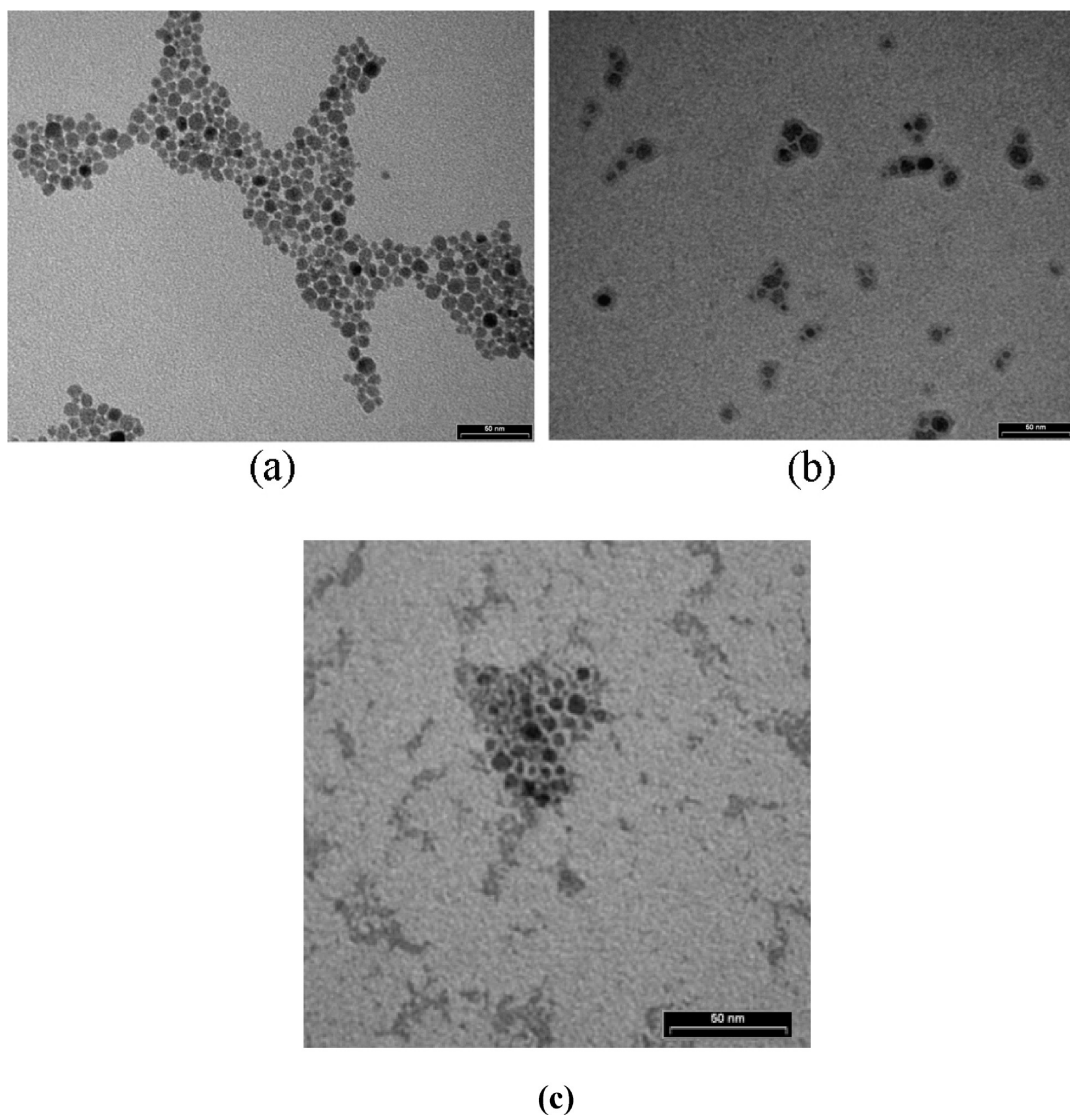


Figure 1. TEM images of (a) bare, (b) SPIONs-COOH, and (c) SPIONs-NH<sub>2</sub>. Bar denotes 50 nm.

**TABLE 1. Sizes Determined by DLS and  $\zeta$ -Potentials in Water of the Different Surface-Modified SPIONs, Presented as Mean  $\pm$  SD over Four Samples**

SPIONs	size (nm)	$\zeta$ -potential (mV)
bare	13.7 $\pm$ 2.1	+43.7 $\pm$ 1.7
CAES-grafted	13.8 $\pm$ 2.1	-15.4 $\pm$ 0.5
APTES-grafted	17.8 $\pm$ 2.6	+32.6 $\pm$ 0.3

The aim of this study was to investigate and compare the cytotoxicity of SPIONs with various surface chemistries on various cell lines (*i.e.*, brain, heart, and kidney) at both cellular and molecular levels. In this case, MTT (3-(4,5-dimethylthiazol-2-yl)-2,5-diphenyltetrazolium bromide) and DNA microarray methods were employed. In addition, we aimed to prove that the cell responses to the same amounts of NPs are significantly dependent on the cell types.

## RESULTS AND DISCUSSION

**Characterization of SPIONs.** Transmission electron micrographs of the bare and surface-modified SPIONs are shown in Figure 1, confirming the formation of SPIONs with a very narrow size distribution. More quantitative size determinations are summarized in Table 1, together with the  $\zeta$ -potentials of the SPIONs in water. There are no significant differences in size of the various SPIONs, whereas  $\zeta$ -potentials in water differ considerably. CAES-grafted particles are negatively charged (SPIONs-COOH), while both bare and APTES-grafted SPIONs are positively charged (SPIONs-NH<sub>2</sub>). Bare SPIONs have a positive surface charge. This last measurement was done on the suspension at acidic pH. Thus, there are  $-\text{OH}_2^+$  on the surface of bare nanoparticles. (At pH 7, we are close to the isoelectric point and the suspension is not really stable.)

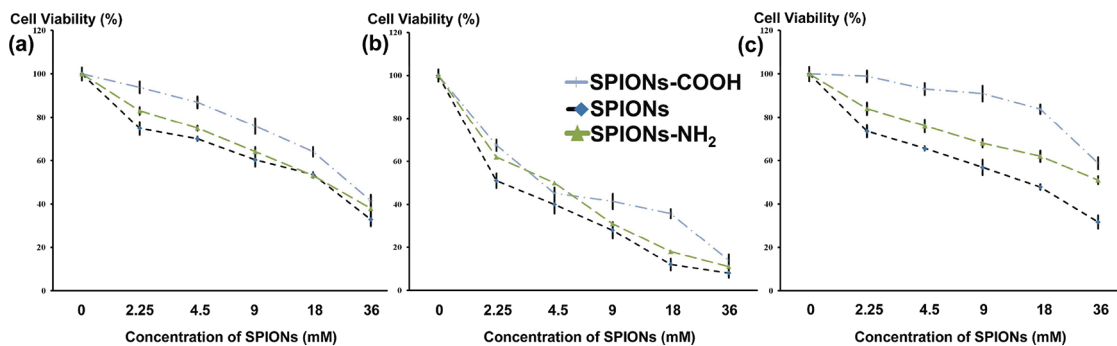


**Figure 2.** Cell viability of MTT assay results for SPIONs-COOH, SPIONs, and SPIONs-NH<sub>2</sub> samples on (a) HCM, (b) BE-2-C, and (c) 293T cell lines.

The number of functional groups on the surface can be estimated at about 2%; the calculation was based on titration as described by Kralj *et al.*<sup>31</sup>

**Physicochemical Effects of SPIONs on Their Toxicity.** **MTT Assay.** MTT reduction was used to metabolically quantify active cells after exposure to the SPION samples. The effect of direct contact of negative, bare, and positive SPIONs with three cell lines was investigated. It is well-recognized that not only the efficacy of SPIONs but also their biomedical fate within cells are strongly dependent on their surface charges.<sup>2</sup> According to the results (Figure 2), positive SPIONs display lower cell viabilities, in all cell lines, in comparison to negative particles.<sup>2</sup> We have previously reported that positive poly(vinyl alcohol)-coated SPIONs with NH<sub>2</sub> terminal groups can escape from endosomes and are released into the cytosol.<sup>2</sup> It is worth noting that, by introducing the positively charged SPIONs into an acidifying lysosomal compartment, the unsaturated amino groups are capable of sequestering protons that are supplied by the proton pump for the digestion of our positive SPIONs. One Cl<sup>-</sup> ion and one water molecule per proton are diffused in the lysosome vesicle.<sup>2</sup> Due to the Coulombic interaction between H<sup>+</sup> and the positively charged SPIONs, more protons will be injected to the lysosome, causing lysosomal swelling and rupture, which leads to nanoparticle deposition in the cytoplasm and the spillage of the lysosomal content. Thus, the reason for the lower cell viability of positive SPIONs may relate to their significant and deep cellular uptake amounts in comparison with negative SPIONs. It is also worth mentioning that the majority of cellular membranes have net-negative charges, causing attractive Coulombic interaction with positively charged SPIONs; this leads to the considerable uptake by cells of positive SPIONs in comparison with negative ones. The above results may explain the observation that the toxicity amounts of bare SPIONs are higher than for other coated SPIONs, due to their tendency to absorb proteins, vitamins, amino acids, and ions causing changes in pH and composition in cells and cell medium.<sup>11,32,33</sup>

**DNA Microarrays. Commonly Altered Genes among Three Model SPIONs.** SPIONs-COOH, SPIONs, or SPIONs-NH<sub>2</sub>

treatment altered the expression levels of 167, 328, or 160 genes, respectively. Among these, 64 genes were altered by two or more chemical treatments (Table 2). Particularly noteworthy was the up-regulation of oxidative stress-inducible genes TXNRD1 coding thioredoxin reductase 1 by the three SPION exposures, HMOX1 coding heme oxygenase 1 by SPIONs-COOH and SPIONs-NH<sub>2</sub> exposures, and the genes associated with glutathione biosynthesis (GCLC and GSR) by SPION exposure.

#### Identification of Genes Specifically Altered by the SPION

**Treatments.** The genes altered specifically in these cell lines under the exposure of SPIONs-COOH, SPIONs, or SPIONs-NH<sub>2</sub> were identified. To further identify genes that would discriminate among the biological actions of SPIONs-COOH, SPIONs, and SPIONs-NH<sub>2</sub>, the genes overlapping among these chemical treatments were excluded. This resulted in a total of 481 genes consisting of 103 SPIONs-COOH specific, 241 SPIONs specific, and 137 SPIONs-NH<sub>2</sub> specific genes, which were used for evaluation of the heavy-metal toxicities.

**Genes Specifically Altered by SPIONs-COOH Treatment.** Of the 103 genes selected to discriminate SPIONs-COOH from SPIONs and SPIONs-NH<sub>2</sub>, 51 were up-regulated and 52 were down-regulated. For further analyses, these genes were functionally classified on the basis of gene ontology (GO). As shown in Figure 3 (and Figure S1, in Supporting Information), 37 up-regulated genes could be annotated and 21 biological processes containing at least three gene hits were found. A particularly important finding was that the SPIONs-COOH treatment induced the genes classified in "M phase", "mitotic cell cycle", "regulation of cell cycle", and "regulation of cell proliferation". These classes contained eight genes (UBE2C, CDC25B, CDKN3, KIF22, H2AFX, SMC4L1, RAE1, and CCNB2), most of which have been reported to be up-regulated in association with acceleration of cell division and proliferation.<sup>34–36</sup> Of these genes, CCNB2, UBE2C, SMC4L1, and CDKN3 exhibited remarkably high fold increases.

On the other hand, the functional classification of 40 annotatable genes repressed by SPIONs-COOH exposure revealed 30 biological processes including

**TABLE 2. Commonly (a) Induced and (b) Repressed Genes among Three Model SPIONs<sup>a</sup>**

(a)			
genes induced	SPIONs-COOH	SPIONs	SPIONs-NH <sub>2</sub>
FOSL1	<b>1.60 (0.0018)</b>	<b>1.56 (0.0021)</b>	<b>1.08 (0.0436)</b>
TXNRD1	<b>1.04 (0.0025)</b>	<b>2.22 (0.0001)</b>	<b>1.03 (0.0405)</b>
PTTG1	<b>3.07 (0.0022)</b>	<b>1.32 (0.0408)</b>	0.77 (0.4891)
AKAP12	<b>2.01 (0.0094)</b>	<b>3.0 (0.0020)</b>	0.10 (0.8617)
KRT19	<b>1.86 (0.0016)</b>	<b>1.79 (0.0015)</b>	0.13 (0.6997)
TLMP1	<b>1.53 (0.0064)</b>	<b>4.45 (0.0001)</b>	0.34 (0.4900)
RBPM3	<b>1.44 (0.0221)</b>	<b>1.90 (0.0064)</b>	0.25 (0.6364)
SPP1	<b>1.43 (0.0334)</b>	<b>1.89 (0.0136)</b>	0.08 (0.9229)
ANXA2	<b>1.38 (0.0046)</b>	<b>2.16 (0.0006)</b>	0.27 (0.7398)
IER2	<b>1.34 (0.0042)</b>	<b>1.06 (0.0062)</b>	0.25 (0.4740)
GLA	<b>1.32 (0.0021)</b>	<b>1.07 (0.0045)</b>	0.48 (0.2745)
SQRDL	<b>1.29 (0.0018)</b>	<b>1.35 (0.0022)</b>	0.24 (0.2590)
LGALS1	<b>1.23 (0.0026)</b>	<b>1.94 (0.0004)</b>	0.05 (0.8897)
HMGA1	<b>1.21 (0.0206)</b>	<b>3.04 (0.0009)</b>	0.84 (0.0745)
SFN	<b>1.17 (0.0459)</b>	<b>1.44 (0.0249)</b>	1.4 (0.0413)
TNFAIP8	<b>1.15 (0.0376)</b>	<b>1.98 (0.0084)</b>	0.78 (0.3243)
TMAP1	<b>1.13 (0.0098)</b>	<b>2.10 (0.0007)</b>	0.06 (0.9129)
GRB10	<b>1.01 (0.0331)</b>	<b>1.11 (0.0246)</b>	0.10 (0.8948)
MAFF	<b>1.00 (0.046)</b>	<b>2.22 (0.0034)</b>	0.14 (0.7957)
HMOX1	<b>1.77 (0.0317)</b>	0.28 (0.6343)	<b>2.47 (0.0114)</b>
TNFAIP3	<b>1.31 (0.0313)</b>	0.68 (0.1513)	<b>1.97 (0.0129)</b>
BHLHB2	<b>1.11 (0.0001)</b>	0.86 (0.0016)	<b>1.41 (0.0178)</b>
VRK2	0.068 (0.0521)	<b>1.07 (0.0049)</b>	<b>2.17 (0.0003)</b>
DUSP1	0.00 (0.9934)	<b>1.24 (0.0206)</b>	<b>3.58 (0.0005)</b>
KLF6	0.96 (0.0005)	<b>1.58 (0.0003)</b>	<b>1.75 (90.0019)</b>
SNFKL	0.49 (0.2852)	<b>1.44 (0.0192)</b>	<b>2.36 (0.0035)</b>
SLC12A6	0.55 (0.1020)	<b>1.00 (0.0107)</b>	<b>1.19 (0.0068)</b>
ETS2	0.41 (0.2006)	<b>1.38 (0.0083)</b>	<b>1.55 (0.0073)</b>
UGCG	0.20 (0.3998)	<b>1.22 (0.0064)</b>	<b>1.23 (90.0096)</b>
PIM1	0.54 (0.4087)	<b>2.06 (0.0250)</b>	<b>2.62 (0.0124)</b>
PIK3CD	0.52 (0.1532)	<b>1.59 (0.0040)</b>	<b>1.06 (0.0171)</b>
KPNA4	0.02 (0.9689)	<b>1.31 (90.0387)</b>	<b>1.50 (0.03589)</b>
TRIB1	0.31 (0.1786)	<b>1.19 (0.0018)</b>	<b>1.31 (0.433)</b>
GCLC	0.31 (0.1002)	<b>2.29 (0.0030)</b>	<b>1.60 (0.0090)</b>
GSR	0.51 (0.1109)	<b>2.21 (0.0020)</b>	<b>1.01 (0.0081)</b>

(b)

genes repressed	SPIONs-COOH	SPIONs	SPIONs-NH <sub>2</sub>
MGAT2	<b>-1.10 (0.0014)</b>	<b>-1.20 (0.0008)</b>	<b>-2.10 (&lt;0.0001)</b>
PGC	<b>-2.05 (0.0001)</b>	<b>-5.19 (&lt;0.000)</b>	-0.93 (0.2754)
AKRIB1	<b>-1.94 (0.0017)</b>	<b>-3.66 (0.0001)</b>	-0.83 (0.4424)
FS	<b>-1.92 (0.0002)</b>	<b>-2.20 (0.0003)</b>	0.33 (0.2524)
CIDEB	<b>-1.85 (0.0002)</b>	<b>-1.49 (0.0003)</b>	-0.44 (0.1725)
F10	<b>-1.81 (0.0002)</b>	<b>-1.10 (90.0045)</b>	-0.11 (0.6383)
GPR30	<b>-1.67 (0.0004)</b>	<b>-2.31 (0.0003)</b>	-0.91 (0.1081)
PGF	<b>-1.64 (0.0027)</b>	<b>-1.19 (0.0063)</b>	-0.31 (0.5551)
GSN	<b>-1.54 (0.0014)</b>	<b>-1.41 (0.0018)</b>	-0.37 (0.4378)
GGCX	<b>-1.54 (0.0005)</b>	<b>-2.44 (0.00001)</b>	-0.55 (0.2430)
VTN	<b>-1.48 (0.0019)</b>	<b>-1.79 (0.000)</b>	0.04 (0.9141)
NUCB2	<b>-1.47 (0.0328)</b>	<b>-1.50 (0.0193)</b>	0.19 (0.7287)
SERPINAS	<b>-1.38 (0.0001)</b>	<b>-2.01 (0.000)</b>	-0.26 (0.4315)
RNP24	<b>-1.34 (0.0048)</b>	<b>-1.23 (0.0037)</b>	0.35 (0.2132)
SERPINAs6	<b>-1.28 (0.0081)</b>	<b>-1.37 (0.0075)</b>	-0.57 (0.2221)

**Table 2. Continued**

genes repressed	SPIONs-COOH	SPIONs	SPIONs-NH <sub>2</sub>
CLPTM1	<b>-1.26 (0.0072)</b>	<b>-1.38 (90.0015)</b>	-0.03 (0.9484)
ADH6	<b>-1.20 (90.0019)</b>	<b>-1.00 (0.0049)</b>	-0.55 (0.0842)
MASK	<b>-1.18 (90.0095)</b>	<b>-1.15 (90.0078)</b>	-0.17 (90.5368)
FURN	<b>-1.18 (0.0288)</b>	<b>-1.06 (90.0463)</b>	0.62 (0.5087)
ACSL1	<b>-1.16 (90.0262)</b>	<b>-1.08 (90.0328)</b>	0.16 (0.8169)
ACP2	<b>-1.10 (90.0200)</b>	<b>-1.32 (0.0120)</b>	0.31 (90.5277)
CX3CL1	<b>-1.07 (0.0054)</b>	<b>-1.14 (0.0043)</b>	-0.44 (0.2607)
SCD	<b>-1.05 (0.0223)</b>	<b>-1.70 (0.0031)</b>	-0.48 (0.2028)
IL17RB	<b>-1.02 (0.0036)</b>	<b>-1.52 (90.0002)</b>	0.01 (90.9811)
ZAPI28	<b>-1.08 (0.0343)</b>	<b>-0.94 (0.0339)</b>	<b>-2.08 (0.0138)</b>
MTIX	0.47 (90.3994)	<b>-1.73 (0.0259)</b>	<b>-2.16 (0.0186)</b>
SFRS1	0.33 (0.2107)	<b>-2.43 (0.0041)</b>	<b>-1.83 (0.0478)</b>
SCAND1	-0.72 (0.0819)	<b>-1.02 (0.0261)</b>	<b>-1.17 (0.0193)</b>
MRPL49	-0.32 (0.2185)	<b>-1.13 (0.0062)</b>	<b>-1.14 (0.0069)</b>
ATP2B1	<b>-1.37 (0.0104)</b>	<b>-1.42 (90.0112)</b>	0.35 (90.2398)
SERPINB1	<b>-1.35 (0.0009)</b>	<b>-1.19 (0.0016)</b>	-0.50 (0.1469)

<sup>a</sup> Numbers in bold indicate expression fold change >2 (log ratio 2) and *p* < 0.05.

"immune response", "lipid metabolism", "amino acid and protein metabolism", and "programmed cell death". These processes contained a total of eight genes (*CLU*, *AZGP1*, *BF*, *TNFSF10*, *PCYOX1*, *BCAT1*, *ALDH6A1*, *PSPH*, *ITIH3*, and *ST6GACNAC4*), all of which exhibited the highest fold transcription decreases.

Since the gene *ALDH6A1* (involved in lipid peroxidation) is down-regulated by SPIONs-COOH, one can expect that lipid peroxidation may be low. According to the gene expression profile, the ROS production might be lower in comparison with SPIONs-NH<sub>2</sub> and SPIONs; however, this must be proven by specific results. The expression of genes associated with cell proliferation and the repression of genes functionally classified in programmed cell death were presumably consequent to the signaling function of low cell content of hydrogen peroxide known to promote cell growth responses.

Table 3 displays the 50 specific genes which are most highly induced and repressed in various cells after interaction with SPIONs-COOH.

**Genes Specifically Altered by SPION Treatment.** Of the 241 genes specifically altered by SPIONs exposure, 114 were up-regulated and 127 were down-regulated. As shown in Figure 3 and Figure S1, these genes were functionally classified into a variety of biological processes. Eighty-five annotatable up-regulated genes were classified into 43 biological processes. Of these processes, programmed cell death and regulation of cell cycle containing 12 genes (*PHLDA2*, *DFFA*, *BCL10*, *CIDE*, *TGFB1*, *CDKN1A*, *NCKAP1*, *FAF1*, *YARS*, *BUB3*, *CHES1*, and *SHC1*), which have been reported to associate with apoptosis or cell growth arrest,<sup>37–40</sup> could be considered to reflect the DNA damaging action of SPIONs. Among these genes, *CDKN1A* (*p21/Waf1*),

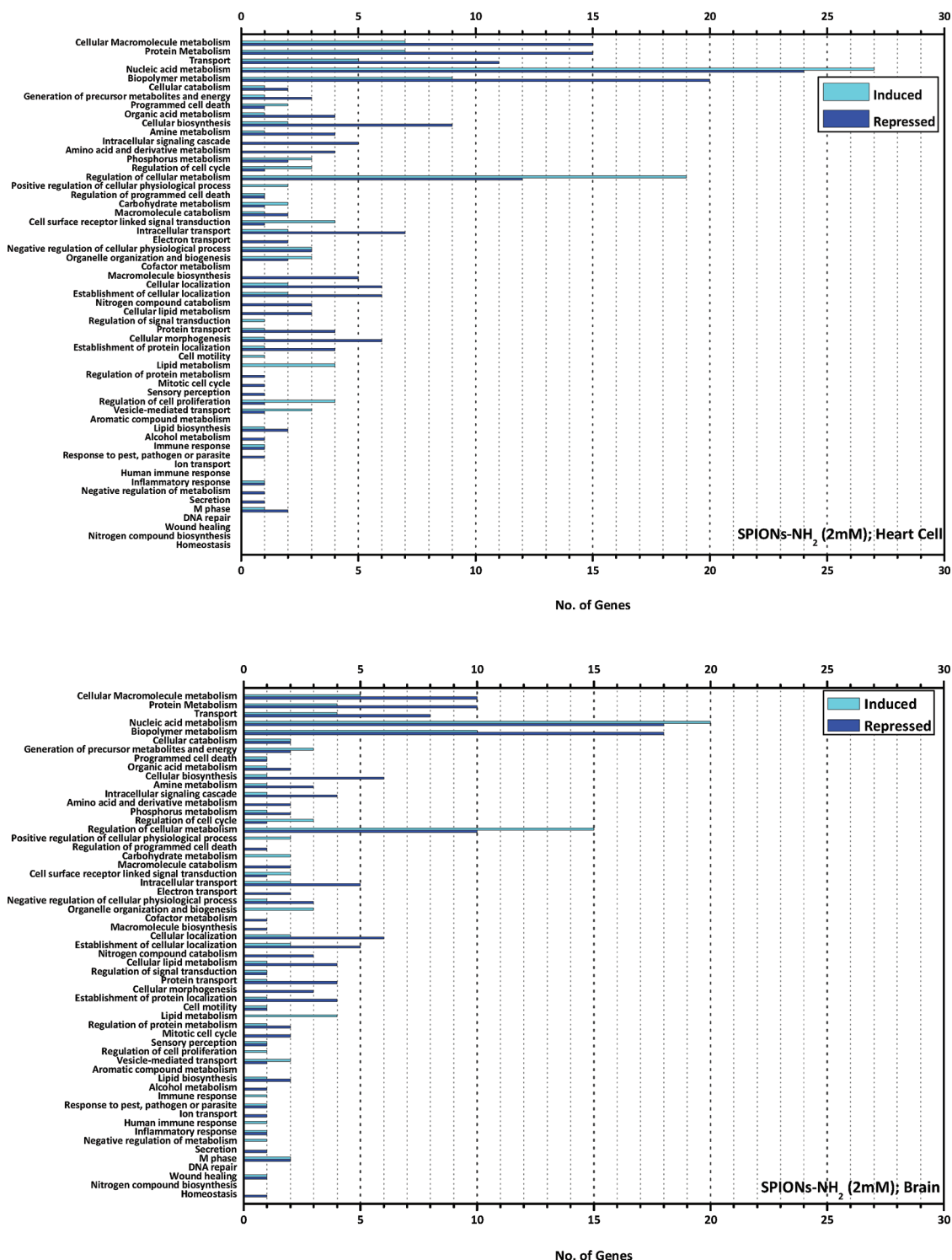


Figure 3. Continued

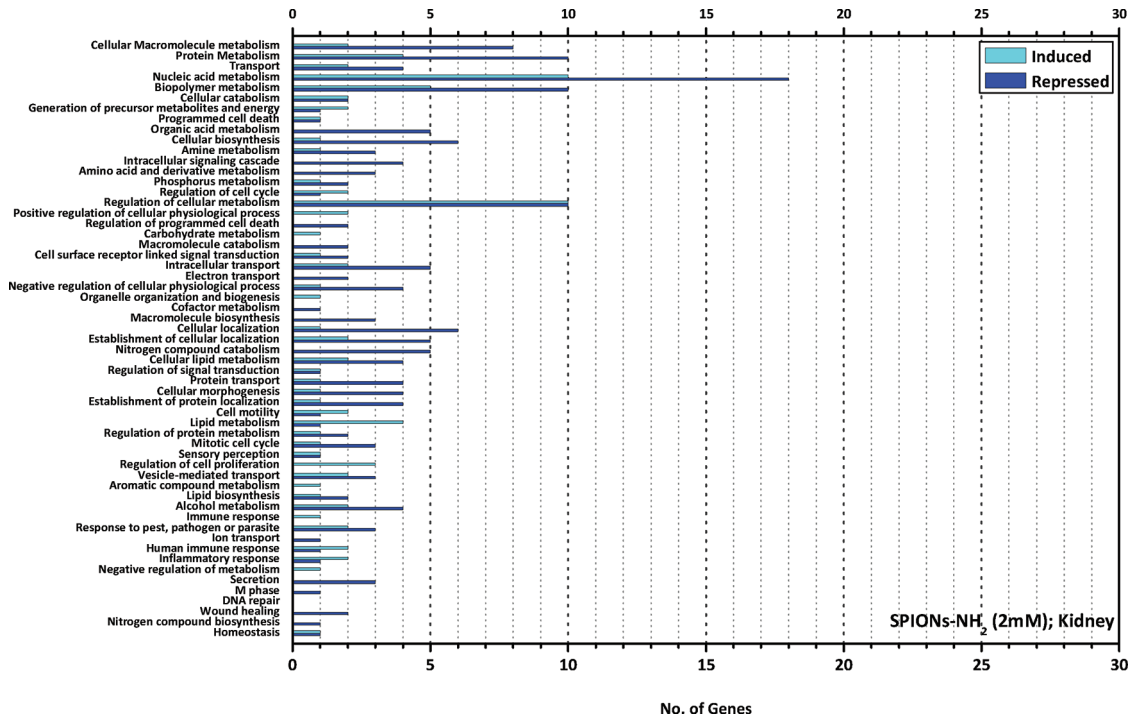


Figure 3. DNA microarray results for incubated HCM, BE-2-C, and 293T cells with 2 mM of positive SPIONs (i.e., SPIONs-NH<sub>2</sub>).

**TABLE 3. Fifty SPIONs-COOH Specific Genes Most Highly Induced and Repressed**

log2-fold change (p value)	
genes induced	genes repressed
CCNB2	2.81 (0.0124)
MCM2	2.67 (0.0037)
UBE2C	2.66 (90.0030)
ZWINT	2.54 (0.0055)
HIST1H4C	2.14 (<0.0001)
RNASEH2A	2.13 (0.0010)
TRIP3	2.04 (0.0004)
PPIH	1.85 (0.0005)
ADM	1.81 (0.0006)
HMGN2	1.81 (0.0027)
RACGAP1	1.67 (0.0021)
TUBA3	1.67 (0.0168)
ITGB3BP	1.62 (0.0002)
SNRPA	1.60 (0.0050)
SMC4L1	1.59 (0.0019)
PC4	1.55 (0.0024)
NUP107	1.55 (0.0015)
TYMS	1.53 (0.0008)
SFRS7	1.52 (0.0065)
CKS2	1.52 (0.0009)
DKK1	1.47 (0.0071)
SFRS2	1.45 (90.0044)
GTPBP6	1.44 (90.0015)
RFC2	1.38 (0.0034)
CDKN3	1.37 (0.0018)
CLGN	-2.22 (0.0023)
OS-9	-2.09 (0.0003)
SERPINC1	-2.04 (0.0001)
TNFSF10	-2.04 (0.0025)
IFRD1	-1.86 (0.0031)
AZGP1	-1.85 (<0.0001)
SLCIA2	-1.75 (0.0014)
ASNS	-1.75 (0.0065)
16.SEP	-1.56 (90.0066)
CALR	-1.50 (0.0027)
GHITM	-1.49 (0.0108)
CDH2	-1.49 (0.0007)
PSPH	-1.49 (0.0086)
ALDH6A1	-1.40 (0.0025)
BCAT1	-1.39 (90.0120)
TST	-1.37 (0.0006)
CLU	-1.37 (0.0003)
EPHX1	-1.37 (90.0206)
BF	-1.35 (0.0088)
C6orf48	-1.34 (0.0007)
ST6GALNAC4	-1.31 (0.0148)
ARSE	-1.26 (0.0001)
ITIH3	-1.25 (0.0111)
TSPAN7	-1.25 (0.0012)
IGSF1	-1.24 (0.0054)

*CIDE*, and *PHLDA2* were remarkably highly up-regulated. Particularly, *CDKN1A* has been shown previously to

**TABLE 4. Fifty SPIONs Specific Genes Most Highly Induced and Repressed**

log2-fold change (p value)	
genes induced	genes repressed
SERPINE2	3.21 (<0.0001)
ABCC3	2.57 (0.0016)
LGALS3	2.30 (0.0012)
GCLC	2.24 (0.0081)
CTSH	2.16 (<0.0001)
AQP3	2.14 (0.0075)
BLVRB	2.14 (0.0026)
HPD	2.14 (0.0005)
CAPN2	2.12 (0.0001)
ENO2	2.07 (0.0001)
GLRX	2.02 (0.0051)
DFNA5	1.95 (0.0005)
PHLDA2	1.95 (0.0007)
HPCAL1	1.91 (<0.0001)
GCNT3	1.89 (0.0015)
CIDE	1.83 (0.0163)
CES1	1.83 (0.0145)
CDKN1A	1.81 (0.0073)
ABCG2	1.69 (0.0027)
STX3A	1.68 (0.0090)
FAH	1.67 (0.0004)
ENPP1	1.66 (0.0143)
ASNS	1.65 (0.0074)
IFTTM2	1.60 (0.0020)
FEZ2	1.60 (0.0001)
UBD	-3.21 (0.0121)
FABP1	-3.16 (0.0006)
CRYAA	-2.95 (0.0047)
EBP	-2.67 (0.0038)
LSS	-2.67 (0.0104)
RELN	-2.59 (0.0012)
PDIA4	-2.54 (0.0015)
HSD17B2	-2.51 (0.0001)
NFKBIA	-2.46 (0.0002)
FDPS	-2.43 (0.0058)
HMGCR	-2.40 (0.0109)
PROM1	-2.36 (0.0021)
SQLE	-2.35 (0.0030)
FDFT1	-2.34 (0.0157)
LIPA	-2.26 (0.0014)
DHCR7	-2.23 (0.0127)
A2M	-2.13 (<0.0001)
ARMET	-2.12 (0.0218)
TRA2A	-2.07 (0.0042)
HSD17B7	-2.02 (0.0016)
C14orf1	-2.01 (0.0323)
ALDH18A1	-1.97 (0.0001)
HMGCS1	-1.93 (0.0407)
NDRG2	-1.92 (0.0006)
PBP	-1.89 (0.0001)

be up-regulated in rat liver treated by DNA damaging agents, such as diethylnitrosamine, and related to

growth arrest following DNA damage.<sup>41–44</sup> It has been reported that SPION treatment increased the frequency of the appearance of micronuclei and sister chromatid exchange in HepG2 cells, and it delayed the cell cycle.<sup>45–48</sup> Our results are consistent with these reports appearing on the list of the 25 genes most strongly repressed.

Table 4 displays the 50 specific genes which are most highly induced and repressed in various cells after interaction with SPIONs.

**Genes Specifically Altered by SPIONs-NH<sub>2</sub> Treatment.** Of the 137 genes specifically altered by SPIONs-NH<sub>2</sub> exposure, 63 were up-regulated and 74 were down-regulated. Functional classification of annotatable genes (43

up-regulated and 55 down-regulated) revealed 14 and 22, respectively, biological processes containing at least three gene hits. As shown in Figure 3 and Figure S1, the genes involved in regulation of cellular metabolism (19 up-regulated and 12 down-regulated) were distinctively altered by SPIONs-NH<sub>2</sub> exposure. This ontology term includes any processes that modulate the frequency, rate, or extent of the chemical reactions and pathways by which individual cells transform chemical substances. Among the genes highly altered, 10 genes are up-regulated (*ING3*, *KLF10*, *MYC*, *ELL2*, *PER2*, *PPARG*, *TCFL5*, *HES1*, *NFYA*, and *TERF2*) and 3 genes are down-regulated (*TAF7*, *RFP*, and *NROB2*). These genes are associated with various processes such as cell proliferation, apoptosis, transcription, abiotic stimulus, and lipid metabolism. Furthermore, the genes associated with cell growth arrest or induction of apoptosis (*ING3*, *TNFRSF21*, *PPM1D*, and *FAS*) were highly up-regulated. These results suggest that SPIONs-NH<sub>2</sub> exposure may affect various cellular functions and particularly may strongly induce cell growth inhibition and apoptosis.

Table 5 displays the 50 specific genes which are most highly induced and repressed in various cells after interaction with SPIONs-NH<sub>2</sub>.

**Effect of Cell Vision.** *MTT Assay.* Figure 4 shows the cell responses to the exact same amount of SPIONs with the same surface chemistries using the MTT assay. The results confirmed the significant differences between cellular responses to the same condition. More specifically, the brain cell is very sensitive to all types of

**TABLE 5. Fifty SPIONs-NH<sub>2</sub> Specific Genes Most Highly Induced and Repressed**

log2-fold change (p value)			
genes induced		genes repressed	
ING3	2.58 (0.0044)	HIS1	-3.13 (0.0031)
KLF10	2.54 (0.0116)	TIMM17A	-2.78 (0.0012)
ID3	2.26 (0.0325)	TAF7	-2.56 (0.0004)
TUFT1	2.17 (0.0002)	TARDBP	-2.51 (0.0175)
BAMBI	1.98 (0.0013)	SS18L2	-2.23 (0.0014)
MYC	1.85 (0.0075)	MCL1	-2.14 (0.0007)
LOC388796	1.83 (0.0116)	RFP	-2.02 (0.0237)
ELL2	1.78 (0.0001)	BLCAP	-2.02 (0.0031)
PER2	1.75 (0.0287)	NROB2	-1.90 (0.0019)
TNFRSF21	1.73 (0.0412)	FBXW2	-1.89 (0.0101)
PELI1	1.72 (0.0113)	HNRPB2	-1.86 (0.0023)
PPM1D	1.66 (0.0065)	SFR55	-1.86 (0.0002)
PPARG	1.59 (0.0033)	DDX3X	-1.85 (0.0006)
DCP1A	1.53 (0.0001)	RAB9A	-1.84 (0.0005)
TCFL5	1.51 (0.0089)	TOB1	-1.78 (0.0005)
TGIF	1.47 (0.0096)	REPIN1	-1.75 (0.0024)
HES1	1.45 (0.0025)	CALU	-1.73 (0.0134)
NFYA	1.45 (0.0058)	PNMA1	-1.72 (0.0124)
FAS	1.43 (0.0011)	RRAGA	-1.69 (0.0033)
CHST3	1.41 (0.0155)	MT1X	-1.65 (0.0290)
SIRT1	1.40 (0.0196)	MAN1A2	-1.61 (0.0004)
GTF3C4	1.40 (0.0193)	PNN	-1.57 (0.0238)
DAZAP1	1.36 (0.0378)	SEPHS2	-1.56 (0.0003)
LRP5	1.36 (0.0095)	MT1H	-1.54 (0.0299)
TERF2	1.35 (0.0026)	CROP	-1.53 (0.0058)

**TABLE 6. Approximate IC<sub>50</sub> Amounts of the Various SPIONs on Different Cells**

cell type	SPION type	IC <sub>50</sub> (mM SPIONs)
HCM	negative SPIONs	30.2
	SPIONs	21.2
	positive SPIONs	22.5
	negative SPIONs	4.3
	SPIONs	2.2
	positive SPIONs	4.5
293T	negative SPIONs	40
	SPIONs	17.1
	positive SPIONs	36

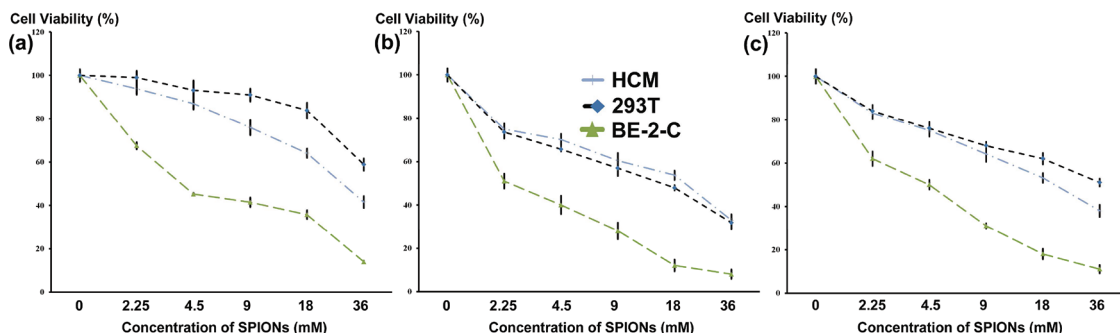


**Figure 4. Cell viability of MTT assay results for (a) SPIONs-COOH, (b) SPIONs, and (c) SPIONs-NH<sub>2</sub> samples on HCM, BE-2-C, and 293T cell lines.**

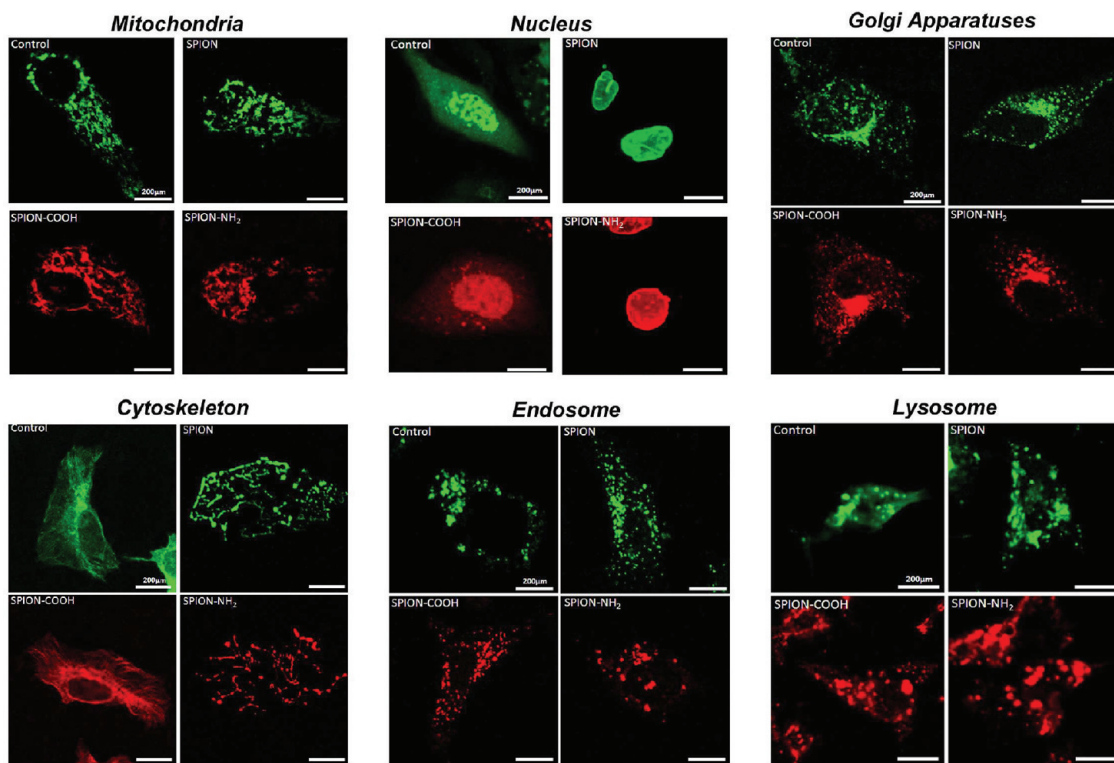


Figure 5. Confocal microscopy images of negative, bare, and positive SPIONs on various cellular compartments of heart cells.

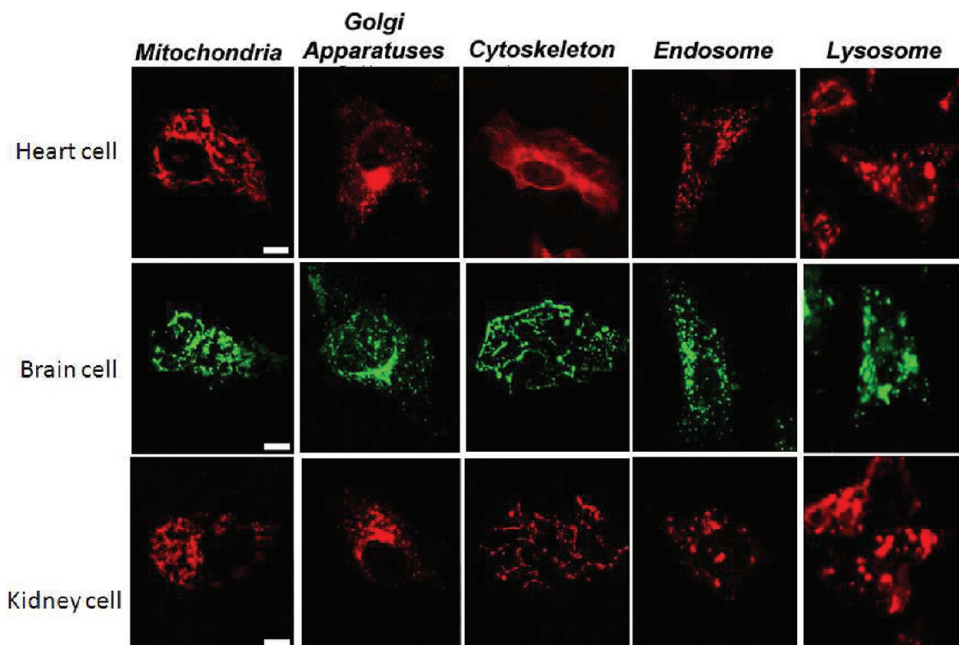
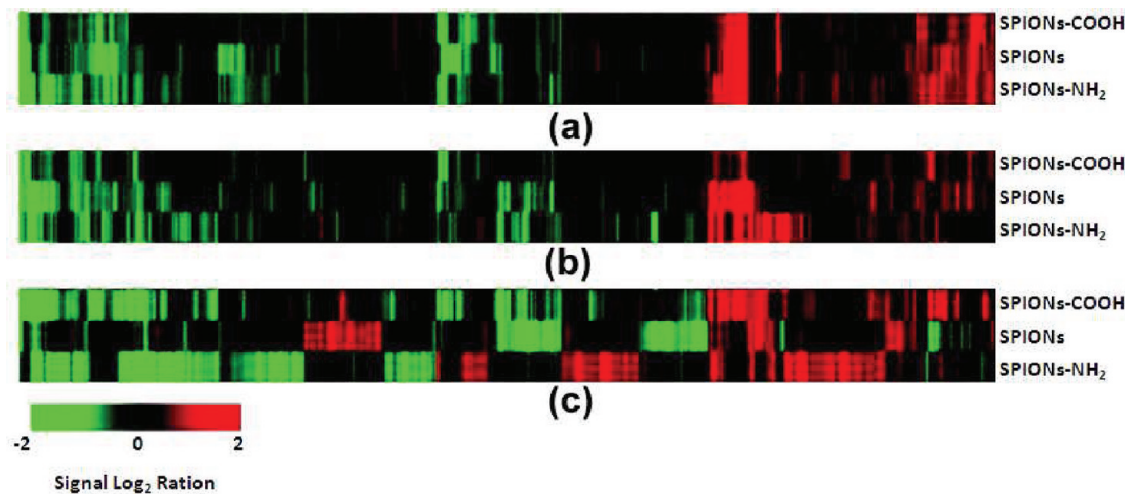


Figure 6. Confocal microscopy images showing the effects of the exact same amount of negative SPIONs on compartments of various cell lines (i.e., heart, brain, and kidney).

SPIONs, whereas heart and kidney cells have the capability to tolerate various SPIONs at higher concentrations. In order to have a better comparison between the physicochemical effects of SPIONs and cell vision, the approximate half-maximal inhibitory concentrations ( $IC_{50}$ ) were defined and are presented in Table 6. The results in Figure 4 and Table 6 confirmed that, in

comparison with the physicochemical effects of SPIONs (see Figure 2), the effect of cell vision on the toxicities at exactly the same concentration of particles is dominant.

**Confocal Microscopy.** HCM cell organelles after 6 h interaction with negative, bare, and positive SPIONs are shown in Figure 5. As seen, the SPIONs-COOH



**Figure 7.** Hierarchical clustering analysis of three model SPION exposures on the basis of 481 genes selected for (a) HCM, (b) BE-2-C, and (c) 293T cell lines. Each row represents one single gene, and each column represents one iron treatment. Red spectrum colors indicate up-regulation, while green spectrum colors indicate down-regulation.

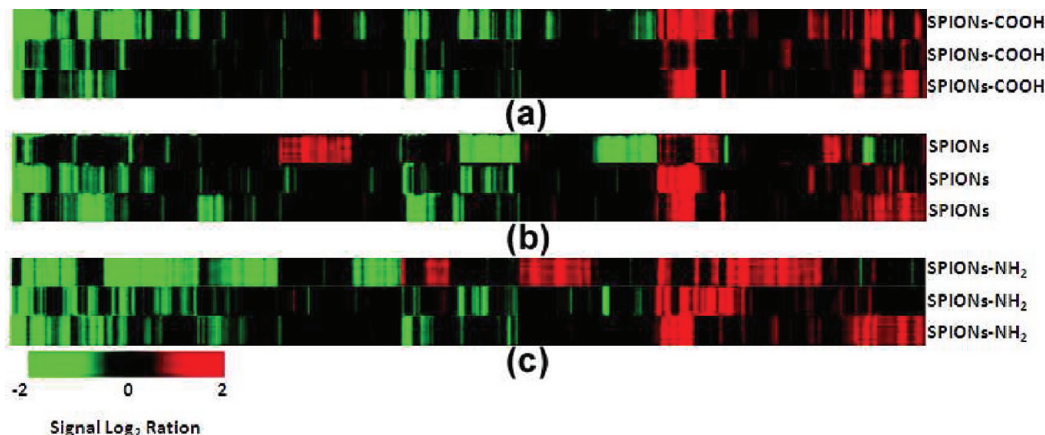


**Figure 8.** Hierarchical clustering analysis of (a) SPIONs-COOH, (b) SPIONs, and (c) SPIONs-NH<sub>2</sub> exposures on the basis of 481 selected genes for all cell lines (i.e., top to bottom of each part: HCM, BE-2-C, and 293T cell lines, respectively). Each row represents one single gene, and each column represents one iron treatment. Red spectrum colors indicate up-regulation, while green spectrum colors indicate down-regulation.

particles exhibit fewer changes in shapes and distribution of cell compartments (e.g., mitochondria, endosome, and lysosome) with respect to the control than the bare and positively charged SPIONs. In order to check the effect of cell vision, the effects of SPIONs-COOH particles on the 3 cell lines were probed (see Figure 6). The results confirm the significant effect of cell vision on the interpretation of the toxic effects of NPs. For instance, negative SPIONs did not produce significant changes on the cytoskeleton of heart cells; in contrast, the exact same amounts of negative SPIONs showed severe toxic effects on the cytoskeleton of both kidney and brain cells.

**Evaluation of SPION Toxicity on the Basis of Expression Patterns of Selected Genes.** In order to visualize the significance of the toxicological effect of cell vision in comparison to the physicochemical properties of SPIONs, a hierarchical clustering analysis was performed. The results are presented as a tree dendrogram (see Figures 7 and 8). The specific

gene alteration and hierarchical clustering revealed that SPIONs-COOH amplified the expression of genes associated with cell proliferative responses. Recent studies have indicated that transition metals cause an increase in the production of ROS, undergoing redox cycle or depleting antioxidants.<sup>49–51</sup> However, this may depend on the surface coating of the SPIONs.

In addition, carcinogenesis is also a well-known effect of heavy-metal toxicity. However, we could not find any relationship between carcinogenesis and the gene expression profiles of SPIONs in our experimental conditions.

Expression of the genes associated with carcinogenesis might be dependent upon exposure time and dose. It has been reported that cadmium chloride, benzo[a]pyrene, and trichloroethylene produced different patterns of gene expression in the livers of exposed mice.<sup>52</sup> Similarly, cadmium chloride, sodium dichromate, and nickel subsulfide altered only a few

**TABLE 7. Fifty SPIONs-NH<sub>2</sub> specific Genes Most Highly Induced and Repressed in the Various Cells**

genes induced	heart	kidney	brain	genes repressed	heart	kidney	brain
ING3	2.58 (0.0044)	0.36 (0.3624)	0.09 (0.8616)	HISI	-3.13 (0.0031)	0.10 (0.6163)	-0.11 (0.5809)
KLF10	2.54 (0.0116)	-0.18 (0.7569)	0.63 (0.2910)	TIMM17A	-2.78 (0.0012)	-0.52 (0.0886)	-0.39 (0.1329)
ID3	2.26 (0.0325)	0.50 (0.5185)	0.49 (0.5278)	TAF7	-2.56 (0.0004)	-0.82 (0.0194)	-0.79 (0.0067)
TUFT1	2.17 (0.0002)	0.26 (0.4198)	-0.14 (0.3344)	TARDBP	-2.51 (0.0175)	0.75 (0.0093)	0.39 (0.0746)
BAMB1	1.98 (0.0013)	-0.23 (0.4077)	-0.09 (0.7223)	SS18L2	-2.23 (0.0014)	0.05 (0.8097)	-0.07 (0.7568)
MYC	1.85 (0.0075)	-0.24 (0.3901)	-0.21 (0.4416)	MCL1	-2.14 (0.0007)	0.64 (0.0223)	0.26 (0.2100)
LOC388796	1.83 (0.0116)	-0.63 (0.2152)	0.44 (0.3556)	RFP	-2.02 (0.0237)	-0.56 (0.0145)	-0.29 (0.1835)
ELL2	1.78 (0.0001)	-0.34 (0.0292)	0.37 (0.0427)	BLCAP	-2.02 (0.0031)	0.00 (0.9989)	-0.18 (0.1779)
PER2	1.75 (0.0287)	-0.08 (0.8878)	-0.13 (0.8161)	NROB2	-1.90 (0.0019)	-0.99 (0.0009)	-1.01 (0.0008)
TNFRSF21	1.73 (0.0412)	0.46 (0.3899)	0.67 (0.2530)	FBXW2	-1.89 (0.0101)	-0.13 (0.6272)	-0.52 (0.1085)
PEL1	1.72 (0.0113)	-1.09 (0.0394)	-1.33 (0.0215)	HNRPH2	-1.86 (0.0023)	-0.29 (0.2988)	-0.62 (0.0393)
PPM1D	1.66 (0.0065)	0.27 (0.0906)	0.12 (0.2010)	SFRS5	-1.86 (0.0002)	0.01 (0.8826)	0.53 (0.0048)
PPARG	1.59 (0.0033)	0.47 (0.0682)	0.49 (0.0703)	DDX3X	-1.85 (0.0006)	-0.49 (0.0632)	-0.28 (0.0491)
DCP1A	1.53 (0.0001)	-0.42 (0.0651)	-0.34 (0.2447)	RAB9A	-1.84 (0.0005)	-0.37 (0.1464)	-0.46 (0.0524)
TCFL5	1.51 (0.0089)	0.50 (0.1904)	0.46 (0.1687)	TOB1	-1.78 (0.0005)	-0.47 (0.0528)	-0.19 (0.5263)
TGIF	1.47 (0.0096)	0.46 (0.1121)	0.18 (0.3616)	REPIN1	-1.75 (0.0024)	-0.49 (0.0011)	-0.44 (0.0032)
HES1	1.45 (0.0025)	-0.10 (0.7273)	0.17 (0.5764)	CALU	-1.73 (0.0134)	0.34 (0.0719)	0.05 (0.7650)
NFYA	1.45 (0.0058)	-0.07 (0.7679)	-0.03 (0.8664)	PNMA1	-1.72 (0.0124)	-0.29 (0.0808)	-0.09 (0.3923)
FAS	1.43 (0.0011)	0.01 (0.9621)	0.34 (0.0972)	RRAGA	-1.69 (0.0033)	0.16 (0.5878)	-0.04 (0.8786)
CHST3	1.41 (0.0155)	0.63 (0.1118)	0.71 (0.0768)	MT1X	-1.65 (0.0290)	0.69 (0.1800)	1.61 (0.0193)
SIRT1	1.40 (0.0196)	0.04 (0.9289)	0.01 (0.9841)	MAN1A2	-1.61 (0.0004)	-0.31 (0.1636)	0.10 (0.5146)
GTF3C4	1.40 (0.0193)	0.95 (0.0426)	0.58 (0.2184)	PNN	-1.57 (0.0238)	0.24 (0.4486)	0.48 (0.1658)
DAZAP1	1.36 (0.0378)	0.32 (0.4549)	0.92 (0.0798)	SEPHS2	-1.56 (0.0003)	-0.35 (0.0497)	-0.42 (0.0052)
LRP5	1.36 (0.0095)	0.40 (0.1604)	0.75 (0.0746)	MT1H	-1.54 (0.0299)	0.79 (0.1253)	1.60 (0.0193)
TERF2	1.35 (0.0026)	-0.53 (0.0229)	-0.24 (0.0689)	CROP	-1.53 (0.0058)	0.72 (0.0235)	0.01 (0.9856)

genes that overlapped with DNA-cross-linker mitomycin C in human lung cells.<sup>53,54</sup> The carcinogenic action of heavy metals might be multifactorial and might not be characterized only on the basis of the genes specifically altered by genotoxic carcinogens, such as DNA-alkylating and DNA-cross-linking agents. Likewise to the MTT results, the variations in the hierarchical clustering for the exact same particles (*i.e.*, both concentration and surface chemistry) and different cells are significantly higher than the variations for the same cell and different particles (*i.e.*, exact same concentration but various surface chemistries). The specific genes that are most highly induced and repressed in various cells are presented in Table 7 and Tables S1 and S2 in Supporting Information. The results show the significant effect of cell “vision”.

## CONCLUSIONS

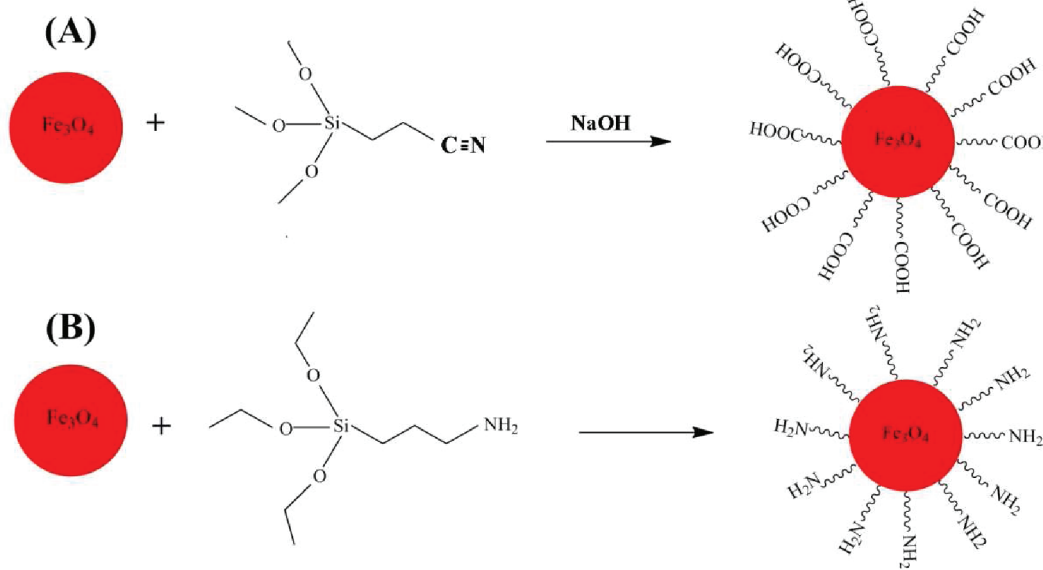
The toxicity of SPIONs with various surface chemistries (bare SPIONs, SPIONs-COOH, and SPIONs-NH<sub>2</sub>)

was evaluated at both cellular and molecular levels. According to the MTT assay, SPIONs-NH<sub>2</sub> display lower cell viabilities in comparison to negative particles, and the toxicity amounts of bare SPIONs are higher than those of other coated SPIONs; SPIONs-COOH, SPIONs, or SPIONs-NH<sub>2</sub> treatment altered the expression levels of 167, 328, or 160 genes, respectively. The specific gene alteration and hierarchical clustering revealed that SPIONs-COOH altered genes associated with cell proliferative responses due to its reactive oxygen species (ROS) properties. In addition to the physicochemical effects of NPs, we found that cell “vision” has significant effects on the obtained toxicity results. Thus, we conclude that the obtained results for specific cells could not be generalized to other cells. The concept of cell vision should be considered in more detail for safe and high-yield design of NPs for biomedical applications and will require serious considerations in the future.

## EXPERIMENTAL SECTION

**Materials.** FeCl<sub>2</sub>·4H<sub>2</sub>O, FeCl<sub>3</sub>·6H<sub>2</sub>O, diethylene glycol, 3-amino-propyltriethoxysilane (APTES), *o*-(2-aminoethyl)-*O*'-methylpolyethylene glycol (PEG-NH<sub>2</sub>, MW = 750), *N*-(3-dimethylaminopropyl)-*N*'-ethylcarbodiimide hydrochloride, tetramethylammonium hydroxide, polyethylene glycol 8000, and *N,N*-dimethylformamide (DMF) were purchased from Sigma-Aldrich. Cynanoethyltrimethoxysilane (CA-ES) was granted by Wacker-Chemie GmbH, Burghausen, Germany.

**Synthesis of SPIONs.** In order to obtain NPs with a narrow size distribution, the polyol method was employed.<sup>55–57</sup> Briefly, 5 mL of an aqueous solution of FeCl<sub>2</sub>·4H<sub>2</sub>O (0.045 M) and FeCl<sub>3</sub>·6H<sub>2</sub>O (0.0375 M) was added to 250 mL of diethyleneglycol. The mixture was heated to 170 °C and maintained at this temperature for 15 min before addition of the base (*i.e.*, solid NaOH (0.375 M)). Subsequently, temperature was maintained at 170 °C for a period of 1 h before cooling to 60 °C. The



Scheme 1. Synthesis route for surface grafting of SPIONs with (A) carboxyl (CAES) and (B) amine (APTES).

TABLE 8. Description of the Cell Lines Used in MTT Studies<sup>a</sup>

cell code	cell type	culture medium
BE(2)-C	human neuroblastoma	1:1 (DMEM + Ham's F12) + FBS10%
HCM	human cardiac myocytes	1:1 (DMEM + Ham's F12) + FBS10% supplemented with 5 $\mu$ g/mL insulin and 50 ng/mL bFGF
293T	human embryonic kidney	RPMI 1640 + FBS10%

<sup>a</sup> DMEM, Dulbecco's modified Eagle's medium; Ham's, nutrient mixture F-10; FBS, fetal bovine serum; RPMI-1640 (Roswell Park Memorial Institute).

synthesized SPIONs were collected with a neodymium magnet and washed with 100 mL of a  $\text{HNO}_3$  (1 M) solution.

In order to obtain functional groups that can react with vectors for targeting, the obtained NPs were coated by suitable polymers (e.g., cynanoethyltrimethoxysilane (CAES) and aminopropyltriethoxysilane (APTES)). Indeed, for molecular imaging, the NPs should be able to target receptors overexpressed in disease thanks to vectors (peptides or mimetic molecules) on their surface.

**Grafting of SPIONs with Cynanoethyltrimethoxysilane.** CAES was grafted on the surfaces of SPIONs, as described elsewhere.<sup>58</sup> Briefly, 100 mL of NP suspension (300 mM iron) was added to 100 mL of DMF, and then 45 mL of 0.15 M CES was slowly added before adding 25 mL of water followed by 15 mL of NaOH solution (1 M) at room temperature and under homogenization (about 8000–24 000 rpm). The solution was heated to 100 °C for 24 h under continuous stirring. The SPIONs were precipitated by addition of an acetone/ether (50/50) mixture and collected with a strong magnet. The precipitate was washed with acetone several times and finally dispersed in water. Excess of silane derivative and other chemicals was removed by dialysis using a dialysis bag (Spectrum Laboratories, Inc.; MWCO = 10 000) for 48 h in water (Scheme 1).

**Grafting of SPIONs with Aminopropyltriethoxysilane.** Briefly, 15 mL of APTES was dissolved in 50 mL of methanol and then dropwise added to a suspension of ferrofluid (20 mL,  $[\text{Fe}] = 0.3$  M) at room temperature. After stirring for 24 h at room temperature, 20 mL of glycerol was added to the mixture and, subsequently, methanol and water were removed by rotary evaporation. Next, 50 mL of acetone was added, and after mixing, the NPs were separated by magnetic decantation. After removing the supernatant, SPIONs were washed several times with acetone. Afterward, the magnetic NPs were dispersed in 40 mL of water and purified by dialysis using a dialysis bag (MWCO = 10 000) for 48 h in water (Scheme 1).

**SPION Characterization: Particle Size Distribution,  $\zeta$ -Potentials, and Transmission Electron Microscopy.** Transmission electron micrographs of the

SPIONs were obtained on a Philips EM 420 (120 kV) by evaporating water from the dispersion on amorphous carbon-coated copper grids. The hydrodynamic diameters and  $\zeta$ -potentials of the SPIONs in water were measured using a Malvern Zeta Sizer Nano S-90 dynamic light scattering (DLS) instrument.

**Cell Description, Cell Culture, and Treatments.** HCM cells from ScienCell Research Laboratories (Carlsbad, CA, USA, Cat #6200) were isolated from the human heart (ventricle). They were cryo-preserved immediately after purification and delivered frozen. HCMs were characterized by the immune fluorescent method with antibodies to myosin. They were guaranteed for further culture at the conditions provided by ScienCell Research Laboratories. The cardiac myocyte was the most physically energetic cell in the body. Its contraction was myogenic (i.e., it is independent of nervous stimulation). All cardiac myocytes were capable of spontaneous rhythmic depolarization and repolarization of their membrane. Cardiac myocyte hypertrophy and apoptosis have been implicated in the loss of contractile function during heart failure. Thus, it is a very good model to analyze the toxicity of three forms of iron nanoparticles (at both cellular and molecular levels) in this cell line.

BE-2-C (ATCC number CRL2268) is a neuroblastoma cell line derived from human bone marrow. The cells are adherent neuroblasts. Human neuroblastoma, the most commonly diagnosed solid tumor in infants, is a cancer of the neural crest. Many of the cell phenotypes characteristic of this transient embryonic structure, particularly neuroblasts, non-neuronal (Schwann, perineurial, or satellite) cells, and even melanocytes, may be present within a single tumor. This property has been used for the classification and prognosis of the disease and, thus, would make it suitable to evaluate the toxicities of this cell line, especially in clinical behavior.

Human embryonic kidney 293T cells, also often referred to as HEK 293, 293T cells, or less precisely as HEK cells, are a specific cell line originally derived from human embryonic kidney. The 293T cells are very easy to grow, transfect very readily, and have been widely used in cell biology research for many years. They

are used also by the biotechnology industry to produce therapeutic proteins and viruses for gene therapy. They are extremely easy to work with and so can be used in experiments in which the behavior of the cell itself is not of interest.

Human HCM (heart), BE-2-C (brain), and 293T (kidney) cell lines were cultured in Eagle's minimal essential medium (MEM) (Nissui, Tokyo, Japan) supplemented with 1% non-essential amino acid (Invitrogen, Carlsbad, CA), 10% fetal bovine serum, and 60 mg/mL kanamycin at 37 °C and 5% CO<sub>2</sub>. Cells were grown to 70% confluence in 60 mm culture dishes and were exposed to 2 mM SPIONs-COOH, SPIONs, and SPIONs-NH<sub>2</sub> for 6 h. This exposure time was selected in order to detect early biological responses, which would be useful indexes for rapid detection of the toxicities of chemicals. The doses were chosen as maximum concentrations at which significant cytotoxicity was not observed (more than 80% cell viability was still determined). Following exposure, cells were washed with phosphate-buffered saline (PBS) and were immediately subjected to RNA extraction. Three independent cultures were used for each treatment or control group.

**MTT Assay.** All cell lines were seeded into a 96-well plate at a density of 10 000 cells (2500 cells for HCM cell line) per well in 100 μL of medium. After 24 h, 40 μL of the corresponding medium containing various concentrations of SPIONs (2–32 mM) was added to each well. Forty microliters of base medium for each cell line was added to negative control wells. All specimens as well as controls were placed in five wells to provide statistically reliable results. The cells were cultured in their specific mediums (see Table 8) and maintained at 37 °C in a 5 and 10% CO<sub>2</sub> incubator.

Cytotoxicity was assessed using the MTT (3-(4,5-dimethylthiazol-2-yl)-2,5-diphenyltetrazolium bromide) assay, which is a nonradioactive, colorimetric technique. Considering the MTT assay, 24 h after the incubation with SPIONs, 100 μL of MTT (0.5 mg/mL) was added to each well. Following incubation, the medium was removed and formazan crystals were solubilized by incubation for 20 min in 150 μL of isopropyl alcohol. The absorbance of each well, which assesses viable cells, was read at 545 nm on a microplate reader (Stat Fax-2100, AWARENESS, Palm City, USA). For the MTT studies, all experiments were carried out in triplicate (*i.e.*, three 96-well plates; 15 repeats total) with the results expressed as mean ± standard deviation; standard deviation values are indicated as error bars in the relevant MTT plots. The results were statistically processed for outlier detection using a "T procedure" in the MINITAB software (Minitab Inc., State College, PA).<sup>59</sup> Statistical differentiations were made by one-way analyses of variance (ANOVA), for which *p* < 0.05 was considered as statistically significant.

**Microarray Experiment.** The cells were lysed directly in culture dishes, and RNA was extracted using RNeasy Mini Kit (Qiagen, Hilden, Germany). Target preparation and hybridization were performed according to one-cycle eukaryotic target labeling assay protocols described in the Affymetrix technical manual (Affymetrix, Santa Clara, CA). cDNA was synthesized from the total RNA by using the one-cycle cDNA synthesis kit (Invitrogen, Carlsbad, CA) with a T7-(dT)24 primer incorporating a T7 RNA polymerase promoter. cRNA was synthesized from the cDNA and biotinlabeled by *in vitro* transcription using the IVT labeling kit (Affymetrix, Santa Clara, CA). Labeled cRNA was fragmented by incubation at 94 °C for 35 min in the presence of 40 mM Tris acetate, pH 8.1, 100 mM potassium acetate, and 30 mM magnesium acetate. Ten micrograms of fragmented cRNA was hybridized to a human genome focus array (Affymetrix, Santa Clara, CA) containing probes for 8795 human genes for 16 h at 45 °C. After hybridization, the microarrays were automatically washed and stained with streptavidin–phycoerythrin by using a fluidics station (Affymetrix, Santa Clara, CA). Finally, probe arrays were scanned with the Genechip System confocal scanner (Affymetrix, Santa Clara, CA).

**Microarray Data Analysis.** Expression data stored as "CEL file" in the GeneChip Operating Software (GCOS) (Affymetrix, Santa Clara, CA) were transferred into the Avadis 4.2 prophetic (Strand Genomics, Redwood City, CA). The signal intensity of probes was scaled and normalized by the MASS algorithm. These summarized data have been deposited at the National Center

for Biotechnology Information (NCBI) Gene Expression Omnibus (GEO; <http://www.ncbi.nlm.nih.gov/geo>) and are accessible through GEO Series accession number GSE6907. To identify differentially expressed genes, unpaired *t* tests for control and respective treatment groups (*n* = 3) were performed for each gene. From the results of these analyses, the genes with *p* < 0.05 and g2.0-fold change in either direction were identified as being differentially expressed. Furthermore, the genes that differentially expressed among the three model chemicals were selected and functionally classified on the basis of gene ontology categories by using the Web-based gene ontology program Fatigo (<http://fatigo.bioinfo.cipf.es>). The hierarchical clustering (using the Euclidean distance metric) analysis and principal component analysis (PCA) were performed on these selected genes using Avadis 4.2.

**Supporting Information Available:** Microarray data for all employed cell types incubated with various SPIONs. Cellular organelle's staining protocols. Software for gene comparisons between various nanoparticles and cell types. This material is available free of charge *via* the Internet at <http://pubs.acs.org>.

## REFERENCES AND NOTES

- Mahmoudi, M.; Hosseinkhani, H.; Hosseinkhani, M.; Boutry, S.; Simchi, A.; Journey, W. S.; Subramani, K.; Laurent, S. Magnetic resonance imaging tracking of stem cells *in vivo* using iron oxide nanoparticles as a tool for the advancement of clinical regenerative medicine. *Chem. Rev.* **2011**, *111*, 253–280.
- Mahmoudi, M.; Sant, S.; Wang, B.; Laurent, S.; Sen, T. Superparamagnetic iron oxide nanoparticles (SPIONs): Development, surface modification and applications in chemotherapy. *Adv. Drug Delivery Rev.* **2011**, *63*, 24–46.
- Laurent, S.; Duts, S.; Hafeli, U.; Mahmoudi, M. Magnetic fluid hyperthermia: Focus on superparamagnetic iron oxide nanoparticles. *Adv. Colloid Interface Sci.* **2011**, *166*, 8–23.
- Mailander, V.; Lorenz, M. R.; Holzapfel, V.; Musyanovych, A.; Fuchs, K.; Wiesneth, M.; Walther, P.; Landfester, K.; Schrezenmeier, H. Carboxylated superparamagnetic iron oxide particles label cells intracellularly without transfection agents. *Mol. Imaging Biol.* **2008**, *10*, 138–146.
- Gupta, A. K.; Naregalkar, R. R.; Vaidya, V. D.; Gupta, M. Recent advances on surface engineering of magnetic iron oxide nanoparticles and their biomedical applications. *Nanomedicine* **2007**, *2*, 23–39.
- Aillon, K. L.; Xie, Y.; El-Gendy, N.; Berkland, C. J.; Forrest, M. L. Effects of nanomaterial physicochemical properties on *in vivo* toxicity. *Adv. Drug Delivery Rev.* **2009**, *61*, 457–466.
- Karlsson, H. L.; Cronholm, P.; Gustafsson, J.; Moller, L. Copper oxide nanoparticles are highly toxic: A comparison between metal oxide nanoparticles and carbon nanotubes. *Chem. Res. Toxicol.* **2008**, *21*, 1726–1732.
- Gupta, A. K.; Berry, C.; Gupta, M.; Curtis, A. Receptor-mediated targeting of magnetic nanoparticles using insulin as a surface ligand to prevent endocytosis. *IEEE Trans. Nanobiosci.* **2003**, *2*, 256–261.
- Gupta, A. K.; Wells, S. Surface-modified superparamagnetic nanoparticles for drug delivery: Preparation, characterization, and cytotoxicity studies. *IEEE Trans. Nanobiosci.* **2004**, *3*, 66–73.
- Mahmoudi, M.; Shokrgozar, M. A.; Simchi, A.; Imani, M.; Milani, A. S.; Stroeve, P.; Vali, H.; Hafeli, U. O.; Bonakdar, S. Multiphysics flow modeling and *in vitro* toxicity of iron oxide nanoparticles coated with poly(vinyl alcohol). *J. Phys. Chem. C* **2009**, *113*, 2322–2331.
- Mahmoudi, M.; Simchi, A.; Imani, M. Cytotoxicity of uncoated and polyvinyl alcohol coated superparamagnetic iron oxide nanoparticles. *J. Phys. Chem. C* **2009**, *113*, 9573–9580.
- Mahmoudi, M.; Simchi, A.; Vali, H.; Imani, M.; Shokrgozar, M. A.; Azadmanesh, K.; Azari, F. Cytotoxicity and cell cycle effects of bare and polyvinyl alcohol coated iron oxide nanoparticles in mouse fibroblasts. *Adv. Eng. Mater.* **2009**, *11*, B243–B250.

13. Hussain, S. M.; Hess, K. L.; Gearhart, J. M.; Geiss, K. T.; Schlager, J. J. *In vitro* toxicity of nanoparticles in BRL 3A rat liver cells. *Toxicol. in Vitro* **2005**, *19*, 975–983.
14. Arbab, A. S.; Bashaw, L. A.; Miller, B. R.; Jordan, E. K.; Lewis, B. K.; Kalish, H.; Frank, J. A. Characterization of biophysical and metabolic properties of cells labeled with superparamagnetic iron oxide nanoparticles and transfection agent for cellular MR imaging. *Radiology* **2003**, *229*, 838–846.
15. Arbab, A. S.; Yocom, G. T.; Wilson, L. B.; Parwana, A.; Jordan, E. K.; Kalish, H.; Frank, J. A. Comparison of transfection agents in forming complexes with ferumoxides, cell labeling efficiency, and cellular viability. *Mol. Imaging* **2004**, *3*, 24–32.
16. Cheng, C. M.; Chu, P. Y.; Chuang, K. H.; Roffler, S. R.; Kao, C. H.; Tseng, W. L.; Sheia, J.; Chang, W. D.; Su, Y. C.; Chen, B. M.; et al. Hapten-derivatized nanoparticle targeting and imaging of gene expression by multimodality imaging systems. *Cancer Gene Ther.* **2009**, *16*, 83–90.
17. Cheng, F. Y.; Su, C. H.; Yang, Y. S.; Yeh, C. S.; Tsai, C. Y.; Wu, C. L.; Wu, M. T.; Shieh, D. B. Characterization of aqueous dispersions of  $\text{Fe}_3\text{O}_4$  nanoparticles and their biomedical applications. *Biomaterials* **2005**, *26*, 729–738.
18. Brunner, T. J.; Wick, P.; Manser, P.; Spohn, P.; Grass, R. N.; Limbach, L. K.; Bruinink, A.; Stark, W. J. *In vitro* cytotoxicity of oxide nanoparticles: Comparison to asbestos, silica, and the effect of particle solubility. *Environ. Sci. Technol.* **2006**, *40*, 4374–4381.
19. Lee, C. M.; Jeong, H. J.; Kim, E. M.; Cheong, S. J.; Park, E. H.; Kim, D. W.; Lim, S. T.; Sohn, M. H. Synthesis and characterization of iron oxide nanoparticles decorated with carboxymethyl Curdlan. *Macromol. Res.* **2009**, *17*, 133–136.
20. Lee, C. M.; Jeong, H. J.; Kim, S. L.; Kim, E. M.; Kim, D. W.; Lim, S. T.; Jang, K. Y.; Jeong, Y. Y.; Nah, J. W.; Sohn, M. H. SPION-loaded chitosan–linoleic acid nanoparticles to target hepatocytes. *Int. J. Pharm.* **2009**, *371*, 163–169.
21. Lee, H.; Lee, E.; Kim, D. K.; Jang, N. K.; Jeong, Y. Y.; Jon, S. Antibiofouling polymer-coated superparamagnetic iron oxide nanoparticles as potential magnetic resonance contrast agents for *in vivo* cancer imaging. *J. Am. Chem. Soc.* **2006**, *128*, 7383–7389.
22. Raty, J. K.; Liimatainen, T.; Wirth, T.; Airenne, K. J.; Ihala, T. O.; Huhtala, T.; Hamerlynck, E.; Vihtinen-Ranta, M.; Narvaren, A.; Yla-Herttula, S.; Hakumaki, J. M. Magnetic resonance imaging of viral particle biodistribution *in vivo*. *Gene Ther.* **2006**, *13*, 1440–1446.
23. Kim, J. S.; Yoon, T. J.; Yu, K. N.; Mi, S. N.; Woo, M.; Kim, B. G.; Lee, K. H.; Sohn, B. H.; Park, S. B.; Lee, J. K.; et al. Cellular uptake of magnetic nanoparticle is mediated through energy-dependent endocytosis in A549 cells. *J. Vet. Sci.* **2006**, *7*, 321–326.
24. Muller, K.; Skepper, J. N.; Posfai, M.; Trivedi, R.; Howarth, S.; Corot, C.; Lancelot, E.; Thompson, P. W.; Brown, A. P.; Gillard, J. H. Effect of ultrasmall superparamagnetic iron oxide nanoparticles (Ferumoxtran-10) on human monocyte-macrophages *in vitro*. *Biomaterials* **2007**, *28*, 1629–1642.
25. Mykhaylyk, O.; Antequera, Y. S.; Vlaskou, D.; Plank, C. Generation of magnetic nonviral gene transfer agents and magnetofection *in vitro*. *Nat. Protoc.* **2007**, *2*, 2391–2411.
26. Lv, G.; He, F.; Wang, X.; Gao, F.; Zhang, G.; Wang, T.; Jiang, H.; Wu, C.; Guo, D.; Li, X.; Chen, B.; Gu, Z. Novel nanocomposite of nano  $\text{Fe}_3\text{O}_4$  and polyalactide nanofibers for application in drug uptake and induction of cell death of leukemia cancer cells. *Langmuir* **2008**, *24*, 2151–2156.
27. Martin, A. L.; Bernas, L. M.; Rutt, B. K.; Foster, P. J.; Gillies, E. R. Enhanced cell uptake of superparamagnetic iron oxide nanoparticles functionalized with dendritic guanidines. *Bioconjugate Chem.* **2008**, *19*, 2375–2384.
28. Horie, M.; Nishio, K.; Fujita, K.; Kato, H.; Nakamura, A.; Kinugasa, S.; Endoh, S.; Miyauchi, A.; Yamamoto, K.; Murayama, H.; Niki, E.; Iwahashi, H.; Yoshida, Y.; Nakanishi, J. Ultrafine NiO particles induce cytotoxicity *in vitro* by cellular uptake and subsequent Ni(II) release. *Chem. Res. Toxicol.* **2009**, *22*, 1415–1426.
29. Wang, A. Z.; Bagalkot, V.; Vasiliou, C. C.; Gu, F.; Alexis, F.; Zhang, L.; Shaikh, M.; Yuet, K.; Cima, M. J.; Langer, R.; et al. Superparamagnetic iron oxide nanoparticle–aptamer bioconjugates for combined prostate cancer imaging and therapy. *Chem. Med. Chem.* **2008**, *3*, 1311–1315.
30. Ge, Y.; Zhang, Y.; He, S.; Nie, F.; Teng, G.; Gu, N. Fluorescence modified chitosan-coated magnetic nanoparticles for high-efficient cellular imaging. *Nanoscale Res. Lett.* **2009**, *4*, 287–295.
31. Kralj, S.; Drofenik, M.; Makovec, D. Controlled surface functionalization of silica-coated magnetic nanoparticles with terminal amino and carboxyl groups. *J. Nanopart. Res.* **2011**, *13*, 2829–2841.
32. Mahmoudi, M.; Simchi, A.; Imani, M.; Shokrgozar, M. A.; Milani, A. S.; Hafeli, U. O.; Stroeve, P. A new approach for the *in vitro* identification of the cytotoxicity of superparamagnetic iron oxide nanoparticles. *Colloid Surf. B* **2010**, *75*, 300–309.
33. Mahmoudi, M.; Simchi, A.; Imani, M.; Milani, A. S.; Stroeve, P. An *in vitro* study of bare and poly(ethylene glycol)-co-fumarate-coated superparamagnetic iron oxide nanoparticles: A new toxicity identification procedure. *Nanotechnology* **2009**, *20*, 225104.
34. Lee, M.; Feinberg, A. Genomic imprinting of a human apoptosis gene homologue, TSSC3. *Cancer Res.* **1998**, *58*, 1052–1056.
35. Nagata, S. Apoptotic DNA fragmentation. *Exp. Cell Res.* **2000**, *256*, 12–18.
36. Barkett, M.; Gilmore, T. D. Control of apoptosis by Rel/NF-B transcription factors. *Oncogene* **1999**, *18*, 6910–6924.
37. Corcoran, C. A.; Huang, Y.; Sheikh, M. S. The p53 paddy wagon: COP1, Pirh2 and MDM2 are found resisting apoptosis and growth arrest. *Cancer Biol. Therapy* **2004**, *3*, 721–725.
38. Tirone, F. The gene PC3TS21/BTG2, prototype member of the PC3/BTG/TOB family: Regulator in control of cell growth, differentiation, and DNA repair? *J. Cell. Physiol.* **2001**, *187*, 155–165.
39. Vairapandi, M. Characterization of DNA demethylation in normal and cancerous cell lines and the regulatory role of cell cycle proteins in human DNA demethylase activity. *J. Cell. Biochem.* **2004**, *91*, 572–583.
40. Yao, X. R.; Scott, D. W. Expression of protein tyrosine kinases in the Ig complex of anti- sensitive and anti-B-resistant B-cell lymphomas: Role of the p55(blk) kinase in signaling growth arrest and apoptosis. *Immunol. Rev.* **1993**, *132*, 163–186.
41. Badie, C.; Dziwura, S.; Raffy, C.; Tsigani, T.; Alsbeih, G.; Moody, J.; Finn, P.; Levine, E.; Scott, D.; Bouffler, S. Aberrant CDKN1A transcriptional response associates with abnormal sensitivity to radiation treatment. *Br. J. Cancer* **2008**, *98*, 1845–1851.
42. Itoh, T.; Linn, S. The fate of p21CDKN1A in cells surviving UV-irradiation. *DNA Repair* **2005**, *4*, 1457–1462.
43. Kabacik, S.; MacKay, A.; Tam, N.; Manning, G.; Finn, P.; Paillier, F.; Ashworth, A.; Bouffler, S.; Badie, C. Gene expression following ionising radiation: Identification of biomarkers for dose estimation and prediction of individual response. *Int. J. Radiat. Biol.* **2010**, *87*, 115–129.
44. Turtoi, A.; Schneeweiss, F. H. A. Effect of 211At particle irradiation on expression of selected radiation responsive genes in human lymphocytes. *Int. J. Radiat. Biol.* **2009**, *85*, 403–412.
45. Kevekorde, S.; Spielberger, J.; Burghaus, C. M.; Birkenkamp, P.; Zietz, B.; Paufler, P.; Diez, M.; Bolten, C.; Dunkelberg, H. Micronucleus formation in human lymphocytes and in the metabolically competent human hepatoma cell line HepG2: Results with 15 naturally occurring substances. *Anticancer Res.* **2001**, *21*, 461–470.
46. Kuo, M. L.; Jee, S. H.; Chou, M. H.; Ueng, T. H. Involvement of oxidative stress in motorcycle exhaust particle-induced DNA damage and inhibition of intercellular communication. *Mutat. Res. Genet. Toxcol. Environ.* **1998**, *413*, 143–150.
47. Lu, Y.; Morimoto, K.; Takeshita, T.; Takeuchi, T.; Saito, T. Genotoxic effects of endosulfan and endosulfan on human HepG2 cells. *Environ. Health Perspect.* **2000**, *108*, 559–561.

48. Uhl, M.; Helma, C.; Knasmuller, S. Single-cell gel electrophoresis assays with human-derived hepatoma (Hep G2) cells. *Mutat. Res., Genet. Toxicol. Environ.* **1999**, *441*, 215–224.
49. Charrier, J. G.; Anastasio, C. Impacts of antioxidants on hydroxyl radical production from individual and mixed transition metals in a surrogate lung fluid. *Atmos. Environ.* **2011**, DOI: 10.1016/j.atmosenv.2010.12.021.
50. Li, Y.; Yang, Z. Y.; Liao, Z. C.; Han, Z. C.; Liu, Z. C. Synthesis, crystal structure, DNA binding properties and antioxidant activities of transition metal complexes with 3-carbaldehyde-chromone semicarbazone. *Inorg. Chem. Commun.* **2010**, *13*, 1213–1216.
51. Li, Y.; Yang, Z. Y.; Wu, J. C. Synthesis, crystal structures, biological activities and fluorescence studies of transition metal complexes with 3-carbaldehyde chromone thiosemicarbazone. *Eur. J. Med. Chem.* **2010**, *45*, 5692–5701.
52. Bartosiewicz, M.; Penn, S.; Buckpitt, A. Applications of gene arrays in environmental toxicology: Fingerprints of gene regulation associated with cadmium chloride, benzo(a)pyrene, and trichloroethylene. *Environ. Health Perspect.* **2001**, *109*, 71–74.
53. Kawata, K.; Yokoo, H.; Shimazaki, R.; Okabe, S. Classification of heavy-metal toxicity by human DIMA microarray analysis. *Environ. Sci. Technol.* **2007**, *41*, 3769–3774.
54. Andrew, A. S.; Warren, A. J.; Barchowsky, A.; Temple, K. A.; Klei, L.; Soucy, N. V.; O'Hara, K. A.; Hamilton, J. W. Genomic and proteomic profiling of responses to toxic metals in human lung cells. *Environ. Health Perspect.* **2003**, *111*, 825–838.
55. Forge, D.; Roch, A.; Laurent, S.; Tellez, H.; Gossuin, Y.; Renaux, F.; Vander Elst, L.; Muller, R. N. *J. Phys. Chem. C* **2008**, *112*, 19178–19185.
56. Mahmoudi, M.; Milani, A. S.; Stroeve, P. Synthesis, surface architecture and biological response of superparamagnetic iron oxide nanoparticles for application in drug delivery: A review. *Int. J. Biomed. Nanosci. Nanotechnol.* **2010**, *1*, 164–201.
57. Mahmoudi, M.; Azadmanesh, K.; Shokrgozar, M. A.; Journeay, W. S.; Laurent, S. Effect of nanoparticles on the cell life cycle. *Chem. Rev.* **2011**, *111*, 3407–3432.
58. Forge, D.; Laurent, S.; Gossuin, Y.; Roch, A.; Vander Elst, L.; Muller, R. N. An original route to stabilize and functionalize magnetite nanoparticles for theranosis applications. *J. Magn. Magn. Mater.* **2011**, *323*, 410–415.
59. Barnett, V.; Lewis, T. *Outliers in Statistical Data*, 3rd ed.; John Wiley and Sons: New York, 1994; pp 584–586.